MICROBIOLOGY

Pf bacteriophages hinder sputum antibiotic diffusion via electrostatic binding

Qingquan Chen[1]†, Pam Cai[2]†, Tony Hong Wei Chang[1], Elizabeth Burgener[3,4], Michael J. Kratochvil[1,5], Aditi Gupta[1], Aviv Hargill[1], Patrick R. Secor[6], Josefine Eilsø Nielsen[7,8], Annelise E. Barron[7], Carlos Milla[3], Sarah C. Heilshorn[5], Andy Spakowitz[2,5]*, Paul L. Bollyky[1]*

Despite great progress in the field, chronic *Pseudomonas aeruginosa* (*Pa*) infections remain a major cause of mortality in patients with cystic fibrosis (pwCF), necessitating treatment with antibiotics. Pf is a filamentous bacteriophage produced by *Pa* and acts as a structural element in *Pa* biofilms. Pf presence has been associated with antibiotic resistance and poor outcomes in pwCF, although the underlying mechanisms are unclear. We have investigated how Pf and sputum biopolymers impede antibiotic diffusion using pwCF sputum and fluorescent recovery after photobleaching. We demonstrate that tobramycin interacts with Pf and sputum polymers through electrostatic interactions. We also developed a set of mathematical models to analyze the complex observations. Our analysis suggests that Pf in sputum reduces the diffusion of charged antibiotics due to a greater binding constant associated with organized liquid crystalline structures formed between Pf and sputum polymers. This study provides insights into antibiotic tolerance mechanisms in chronic *Pa* infections and may offer potential strategies for novel therapeutic approaches.

INTRODUCTION

Cystic fibrosis (CF) is a life-shortening disease marked by chronic pulmonary infections, inflammation, and structural damage of the lung tissue (*1*). The absence or dysfunction of the epithelial CF transmembrane conductance regulator (CFTR) protein leads to a buildup of viscous mucous in the airways (*2*). While CFTR modulator therapy has improved outcomes significantly for people with CF (pwCF) in many ways, infections remain problematic (*3*).

Pseudomonas aeruginosa (*Pa*) is the most common pathogen in bacterial lung infections by adulthood for pwCF. Chronic endobronchial infection with *Pa* is associated with poor lung function, increased pulmonary exacerbations, and increased mortality (*4*–*7*). While *Pa* eradication protocols are now standard of care, success is unfortunately variable and not sustained (*8*, *9*). Nearly 60% of patients will have chronic *Pa* infection by their mid-20s (*2*). Despite the advent of CFTR modulator therapy, chronic *Pa* infections remain an important problem in CF (*10*).

Tobramycin (TOB) is the most common inhalational antibiotic used to treat chronic *Pa* infections, although other antipseudomonal antibiotics are often used (*11*). However, clinical responses to antibiotics in pwCF are frequently variable and not necessarily predicted by antibiotic susceptibility testing data (*12*–*14*). Therefore, there is great interest in identifying factors that affect antibiotic efficacy in CF.

We and others have identified a role for Pf bacteriophages—a virus that infects *Pa*—in *Pa* pathogenesis and susceptibility to antibiotics. Pf phages are filamentous bacteriophages of the Inovirus family (*15*, *16*) that are widespread across *Pa* isolates (*17*–*19*). Unlike most phages that parasitize bacteria (*20*, *21*), filamentous phages such as Pf are pseudolysogenic—they do not require the lysis of their bacterial hosts to release infectious virions (*22*). Instead, virions are extruded from the cell envelope of *Pa* without lysis. There are indications that Pf may enhance *Pa* fitness (*23*, *24*) and promote *Pa* biofilm formation (*25*). *Pa* biofilms that include Pf phages contain liquid crystalline regions with alignment of the Pf filaments (*26*, *27*) driven by depletion attraction forces between Pf phages and polymers (*24*). Pf mixed with polymers present during *Pa* infection, such as DNA or hyaluronic acid, rapidly assembles into thick, adherent, birefringent biofilms (*26*), indicating that the liquid crystalline state seen in *Pa* biofilms stems from interactions between Pf phages and polymers.

Pf phage is associated with more severe disease exacerbations in pwCF (*28*) and chronic wound infections (*29*). Pf also reduces antibiotic efficacy (*30*) as Pf mixed with polymers typically found in human sputum increased *Pa* tolerance to TOB, gentamicin, and colistin (COL) (*26*). Moreover, Tarafder *et al.* (*31*) showed visually how Pf phages form occlusive sheaths around *Pa* that shield them from antibiotics. Phage-mediated polymer organization is particularly relevant to the pathophysiology of CF airway infections, where dense, polymer-rich secretions in the airways create ideal conditions for liquid crystal formation.

The mechanism underlying how Pf phages hinder antibiotic efficacy is unclear. Recent work showed that the association of filamentous phage–containing tactoids with *Pa* has a negative effect on antibiotic efficacy (*26*, *31*, *32*), but the relative contribution of the association of phage or sputum polymers with antibiotics is not well studied and likely plays a critical role in lowering antibiotic efficacy. Rossem *et al.* (*33*, *34*) proposed a mathematical model wherein antibiotic diffusion through a single liquid crystalline tactoid, formed by Pf phages and polymers and encapsulating a bacterium, is limited by the adsorption of antibiotics to Pf phages. While the general trend of their modeling agreed with previously published data on antibiotic and phage interactions, we sought to perform a more direct comparison between experimental and model results to illuminate

[1]Division of Infectious Diseases and Geographic Medicine, Dept. of Medicine, Stanford University School of Medicine, Beckman Center, 279 Campus Drive, Stanford, CA 94305, USA. [2]Department of Chemical Engineering, Stanford University, Stanford, CA, 94305, USA. [3]Center for Excellence in Pulmonary Biology, Department of Pediatrics, Stanford University, Stanford, CA 94305, USA. [4]Children's Hospital of Los Angeles, Keck School of Medicine, University of Southern California, Los Angeles, CA 90027, USA. [5]Department of Materials Science and Engineering, Stanford University, 476 Lomita Mall, Stanford, CA 94305, USA. [6]Division of Biological Sciences, University of Montana, Missoula, MT 59812, USA. [7]Department of Bioengineering, School of Medicine & School of Engineering, Stanford University, Stanford, CA 94305, USA. [8]Department of Science and Environment, Roskilde University, 4000 Roskilde, Denmark.
*Corresponding author. Email: pbollyky@stanford.edu (P.L.B.); ajspakow@stanford.edu (A.S.)
†These authors contributed equally to this work.

the underlying mechanisms and exact contribution of each sputum component. Thus, in addition to our experimental observations, we also developed a set of continuum models for the entire sputum environment (encompassing tactoids that can form within) to hypothesis test potential mechanisms.

In this work, we have asked how Pf phages interact with commonly used inhaled antibiotics, such as TOB, in a novel model system incorporating sputum samples and sputum polymers. Using fluorescent recovery after photobleaching (FRAP), calorimetry, and mathematical modeling, we show that Pf inhibits antibiotic diffusion via charge-based interactions. These findings may help guide the selection of inhaled antibiotics and inform potential therapies directed at Pf phages.

RESULTS

TOB diffusion is impaired in Pf-positive sputum

We sought to define the impact of Pf phages on antibiotic diffusion in sputum. To this end, TOB was fluorescently labeled using Cy5 and homogenously mixed with sputum. We then used FRAP, a technique where a laser is used to photobleach an area of the sputum mixture. After photobleaching, the fluorescence recovery of the bleached area is measured as a function of time as fluorescent particles diffuse from outside the bleached area into the bleached area (Fig. 1A). We obtained a fluorescence recovery curve from FRAP, which allows understanding of the diffusion rate of the fluorescently tagged particle within the medium.

To assess the impact of Pf phages on TOB diffusion, we collected sputum samples from three pwCF who had *Pa* infections but had no Pf detected in the sputum sample by quantitative polymerase chain reaction (Pa^+Pf^-). Pf status was determined using a protocol previously reported by our group (*19*) (table S1). Half of these samples were spiked with Pf phage (Pa^+Pf^+). We observed that the fluorescence of TOB in the bleached region after 3 min was substantially lower in Pa^+Pf^+ sputum compared to Pa^+Pf^- sputum (Fig. 1B and fig. S1 and S2). The time window of 3 min was chosen because TOB in pure phosphate-buffered saline (PBS) reaches full fluorescence recovery by this time. The apparent diffusion coefficient (tau^{-1}), which gives an average rate of particle diffusion in the fluid, was also found to be lower in the case of Pa^+Pf^+ sputum (Fig. 1C), indicating slower TOB diffusion in the presence of Pf. On the other hand, ciprofloxacin (CIP), which has a neutral charge, fluorescently labeled using Cy5 (Cy5-CIP) displayed the opposite trend in diffusion (Fig. 1D). The FRAP recovery curves from which the diffusion coefficients were derived further support the marked decrease in diffusion of Cy5-TOB when Pf is present (fig. S2A) compared to Cy5-CIP (fig. S2B).

Pf phages inhibit the diffusion and efficacy of TOB in sputum polymers

We then sought to interrogate how Pf affects the diffusion and efficacy of TOB in more controlled systems. To this end, we studied a set of antibiotics against PA14: TOB, COL, CIP, and aztreonam (AZT). Because sputum is highly heterogenous and variable from patient to patient, to facilitate reproducible mechanistic analyses of phage/polymer/antibiotic interactions, we made simple sputum by combining DNA (4 mg/ml) and mucin to 8% solids (w/w) for these studies (*26*). Notably, we did not include the amino acids, lipids, egg yolk, etc. that are often incorporated into artificial sputum preparations (*35*) to primarily focus on the interaction between sputum

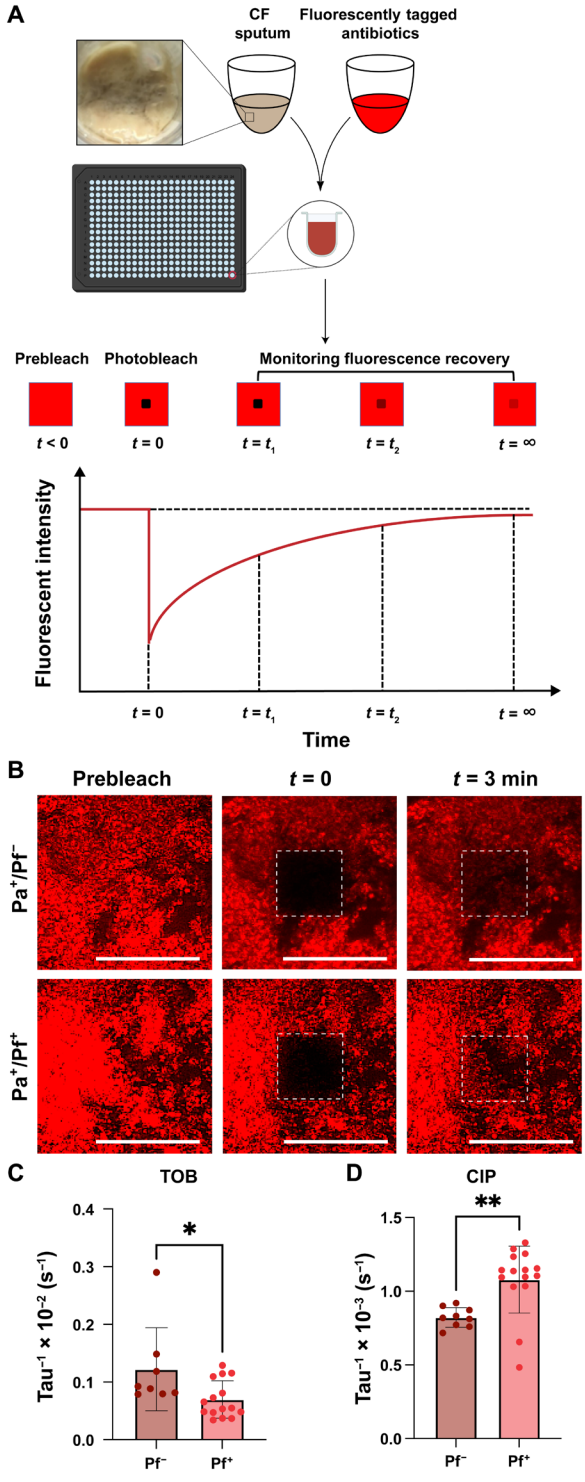

Fig. 1. TOB diffusion is decreased in Pf-positive sputum. (**A**) FRAP was adopted to determine the diffusion of Cy5-TOB in sputum samples collected from patients with CF. (**B**) FRAP was used to measure the recovery intensity of Cy5-TOB after photobleaching in sputum collected from patients with CF. The effective diffusion coefficient (tau^{-1}) of (**C**) Cy5-TOB and (**D**) Cy5-CIP in three patient sputum samples supplemented with Pf (Pf^+; $n = 15$ for TOB and $n = 9$ for CIP) phages was less compared to Pf-negative (Pf^-; $n = 10$ for TOB and $n = 15$ for CIP)–expectorated CF sputum. Unpaired *t* test, $*P \leq 0.05$, $**P \leq 0.01$. Scale bar, 200μm.

polymers and Pf. However, in artificial sputum containing these other reagents, we observe similar trends (fig. S3).

We first examined the impact of Pf phages and sputum polymers on bacterial killing. We found that the combination of Pf phages and sputum polymers resulted in a highly statistically significant decrease in bacterial killing for TOB (Fig. 2A) and COL (fig. S4A) but not for CIP (Fig. 2A) and less statistically significantly for AZT (fig. S4A). From here, we decided to focus on TOB and CIP due to their similar size and respective charges (i.e., TOB is positive, and CIP is neutral), making them good contrasting molecules to investigate one physical mechanism of antibiotic tolerance in the presence of Pf. We acknowledge that TOB, an aminoglycoside, and CIP, a fluoroquinolone, exhibit different mechanisms of action against *Pa*.

We then used FRAP to quantify the diffusion rate of Cy5-TOB and Cy5-CIP in sputum polymers. In fig. S5 (A and B), the fluorescent recovery curve is shown for Cy5-TOB and Cy5-CIP, respectively. The effective diffusion rate, found by assuming that the fluorescent recovery is due purely to Fickian diffusion, is given by tau^{-1} (with units per second), whose value for each condition is plotted for Cy5-TOB and Cy5-CIP in Fig. 2 (B and C, respectively). Comparing the effective diffusion rates of TOB and CIP with the condition of having both Pf phages and simple sputum present, we found that the combination of Pf and simple sputum resulted in a significantly decreased fluorescence recovery for TOB (Fig. 2B and fig. S5A) but less so for CIP (Fig. 2C and fig. S5B). Additional comparison statistics support that TOB exhibited sharper drops in diffusion rate due to Pf and simple sputum (fig. S6, A and B). Together, these data suggest that Pf and sputum polymers (DNA and mucin) have distinct effects on the diffusion of different antibiotics.

Isothermal titration calorimetry results support electrostatics as the driving force in TOB sequestration by Pf phages and sputum biopolymers

To interrogate the mechanism underlying decreased antibiotic efficacy in the presence of Pf phages, we assessed the interaction strength between Pf and antibiotics using isothermal titration calorimetry (ITC). Because TOB is a highly positively charged molecule at physiological pH (table S2) (*36*), we hypothesized that negatively charged Pf and sputum polymers would reduce the diffusion of positively charged antibiotics due to electrostatic attraction, diminishing antimicrobial efficacy. This hypothesis is supported by the differences in the effective diffusion coefficient (tau^{-1}) between TOB and CIP (Fig. 2, B and C, and fig. S6, A and B) across the conditions of Pf, mucin and DNA, and all the above. While there is a significant drop in tau^{-1} from antibiotic alone to either Pf or sputum polymers present for both antibiotics, the statistically significant drop in tau^{-1} between Pf only and Pf + mucin + DNA in TOB (Fig. 2B and fig. S6A) but not CIP(Fig. 2C and fig. S6B) could be defined by their differing electrostatic natures. For these assays, we used only Pf and DNA to focus on this specific interaction in the measurement. TOB or CIP was titrated into solutions of either Pf phages, DNA, or both. The heat released from titrating in TOB to each solution was mostly positive (Fig. 3A), which corresponds to an energetically favorable interaction between TOB and Pf and DNA. On the other hand, the heat released from titrating CIP into each solution was mostly negative (Fig. 3B), indicating that the energy was consumed and the mixing is energetically unfavorable. The heat released from titrating each antibiotic into Pf or Pf with mucin showed very little effect of mucin on thermodynamic values (fig. S7).

To quantitatively derive the strength of interaction between antibiotics and polymers from the isotherms, we fit a thermodynamic model to the isotherms that accounts for thermodynamic contributions from excess entropy associated with electrostatic interaction and enthalpy of phase changes such as coacervation. The model is based on basic polymer physics principles and is described in more detail in Materials and Methods. This model has previously been used to analyze binding mechanisms in polyelectrolyte solutions composed of equal concentrations of oppositely charged polymers, which will first pair up electrostatically in solution before phase

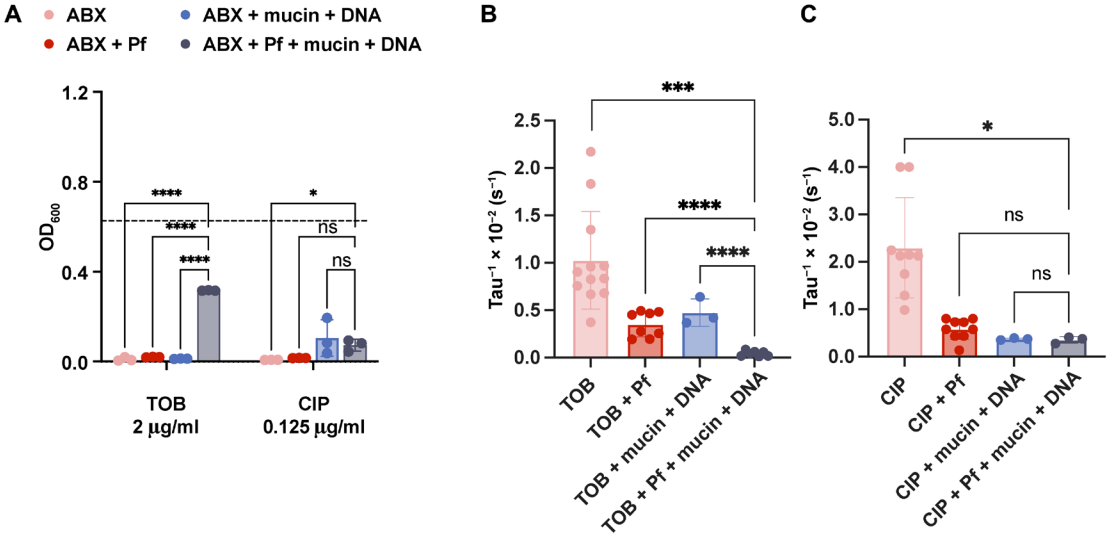

Fig. 2. Pf and sputum polymers affect the efficacy and diffusion of TOB but not CIP. (**A**) To assess the impact of filamentous bacteriophages (Pf) and lung polymers on antibiotic efficacy, we measured TOB and CIP killing of *Pa* ($n = 3$). ABX, antibiotics. Dashed line indicates optical density (OD) of bacteria grown in control medium. The effective diffusion rate, tau^{-1}, was plotted for (**B**) Cy5-TOB in PBS ($n = 12$), Pf ($n = 10$), mucin and DNA ($n = 3$), and Pf with mucin and DNA ($n = 7$). The effective diffusion rate is shown for (**C**) Cy5-CIP in PBS ($n = 9$), Pf ($n = 9$), mucin and DNA ($n = 3$), and Pf with mucin and DNA ($n = 3$). $^*P \leq 0.05$, $^{***}P \leq 0.001$, and $^{****}P \leq 0.0001$, (A) two-way analysis of variance (ANOVA) for OD_{600} and [(B) and (C)] unpaired *t* test for tau^{-1} plots. ns, not significant.

separating into coacervates (*37*). In our case, the assumption is that electrostatic attraction between positively charged antibiotics and negatively charged Pf and DNA would drive the process of ion pairing. If enough charged species bind together past a certain threshold, there could be phase separation of the complex of antibiotics, Pf, and DNA out of the solution. Cloudiness was observed in the chamber after titrating TOB into Pf and DNA, indicating that a phase change had occurred (fig. S8).

Using the model, the binding affinity and the enthalpy change of the ion pairing process were determined (figs. S9 and S10). The binding affinity, K_a, gives insight into the strength of interaction between the antibiotic and polymers in the solution, with higher values indicating that more antibiotics and polymers are bound at equilibrium (Fig. 3C). Consistent with our predictions, the positively charged TOB exhibited much greater binding affinity with DNA, Pf, and the DNA + Pf mixture than the neutrally charged CIP under each condition (Fig. 3D).

In addition, the binding affinity can be used to calculate free energy change due to the ion pairing process, composed of energetic and entropic contributions. A greater positive change in the entropic contribution correlates to more binding (Fig. 3E). We observed a greater negative entropic contribution to the free energy change for neutrally charged CIP than the positively charged TOB (Fig. 3F). The more positive entropic change due to the ion pairing between oppositely charged TOB and sputum components (Pf phages and DNA) compared to CIP is in line with what has previously been found in oppositely charged polyelectrolyte mixtures (*37*–*39*), suggesting that TOB interacts with sputum components in a charge-dependent manner. For TOB binding to DNA, we found that the entropy change is 12.56 cal/mol·K, which is just above but comparable to the range that previous work found for DNA and the above three multivalent ions (*40*). The higher entropy value indicates that TOB binding to DNA is even more favorable than the above mentioned ions and is a largely entropically driven process.

Together, the data indicate that TOB but not CIP binds to both Pf phages and DNA and implicates electrostatic interactions as the driving force. Notably, we did not observe substantial differences in the binding affinities between TOB in Pf alone and in the Pf + DNA mixture (Fig. 3D). This suggests that binding strength cannot explain the decrease in TOB diffusion in the presence of Pf and DNA and that higher-order interactions between Pf phage and DNA (e.g., the ability of Pf to organize DNA into a crystalline network) may play a crucial role.

DNA and Pf phages hinder the diffusion of TOB in a pH-dependent manner

We sought to assess the impact of pH in these interactions. Because pH changes could be expected to alter a molecule's effective charge, altering pH allowed us to assess the impact of electrostatic forces. We repeated the bacterial killing assay in Fig. 2, using only DNA and Pf phage. We found that mixtures of TOB and DNA but not CIP and DNA reduce bacterial killing (Fig. 4A). We also find that TOB and Pf slightly reduce bacterial killing, which agrees with previous findings (Fig. 4A) (*26*, *31*). We then repeated these studies over a range of pH values. Bacterial growth was not affected until the pH was above 10. We found that the efficacy of TOB was restored as the pH increased above 7 (Fig. 4B) because the amide groups in TOB at higher pH values undergo deprotonation (*41*), thereby decreasing the positive charge on the molecule. The pH dependence of TOB antimicrobial activity indicated that the charged interactions between Pf phage, DNA, and TOB affect TOB efficacy. In contrast, the antimicrobial activity of CIP was not significantly affected by pH (Fig. 4C).

In parallel, FRAP experiments were performed to determine the diffusion of antibiotics through DNA, Pf phages, and mixtures of DNA and Pf phages at pH 7. As expected, on the basis of previous studies, we observed colocalization of Cy5-TOB within the liquid crystal tactoids formed in mixtures of DNA and Pf phages (Fig. 4E) (*26*). The fluorescent recovery decreased as more components were added to the solution (fig. S11A). Cy5-TOB (pink curve), by itself, recovered fully. Adding Pf phages (red curve) or DNA (blue curve) slowed the effective diffusion rate, tau^{-1}, but combining both (black curve) slowed the diffusion even further (Fig. 4D). The diffusion of Cy5-CIP was not affected by the presence of both Pf and DNA (figs. S11B and S12). Together, the results for bacterial killing at varying pH and FRAP curves implicate electrostatic forces in TOB affinity for and inactivation by Pf phage and DNA.

We also interrogated the alternative hypothesis that increased quantities of macromolecules were decreasing the mesh size to be smaller than the size of the antibiotic molecule and limiting diffusion by being a physical barrier. To test this, we used fluorescein isothiocyanate–dextran molecules of the same order of magnitude in size as TOB to investigate whether changes in mesh size would limit antibiotic diffusion. We found that the mesh size did not change because of the addition of Pf and DNA, as the fluorescein isothiocyanate–dextran molecule exhibited similar diffusion rates under all conditions with sputum components (fig. S13).

In modeling studies, higher-order structures formed by DNA and Pf phages reduce the diffusion of charged antibiotics through electrostatic interactions

We sought to understand better the binding interactions that underlie TOB sequestration through modeling studies. To model this transient binding that can occur and its effect on fluorescent recovery in an FRAP experiment, we derived a two-state model that assumes that the antibiotic molecule transiently switches between a free state and being bound to another constituent (Fig. 5D). The model contains binding and unbinding rates, which govern the kinetics of the associations, as well as a parameter α, which is the ratio of the diffusion in the bound state to the diffusion in the free state. A detailed derivation and description of this model can be found in Materials and Methods. We note that the model assumes that the presence of bacteria and their activity with antibiotics are negligible. The two-state model was fit to FRAP data for both TOB (Fig. 5A) and CIP (Fig. 5B) diffusions in Pf phages to determine the kinetics of the binding to Pf phages and the relative decrease in diffusion related to binding (Fig. 5, A and B, blue curves). We similarly fitted the two-state model to our FRAP data for TOB and CIP diffusions in DNA alone (Fig. 5, A and B, red curves).

In the case where both Pf phages and DNA are present in the solution, we hypothesized that the diffusion of antibiotics should be a function of antibiotics in three states: free diffusion, bound to Pf phages, and bound to DNA (Fig. 5E). To model this scenario, we derived the three-state model that includes kinetic parameters to govern the transitions among these three states and ratios of the relative diffusion rates in each state (described in detail in Materials and Methods). In this noncooperative three-state model, we assume that the binding of antibiotics to DNA is independent of the binding of antibiotics to Pf phage. Thus, we can use the parameters we derived for antibiotic diffusion in DNA alone and Pf phages alone from fitting the two-state model to these scenarios to generate a predicted diffusion curve with

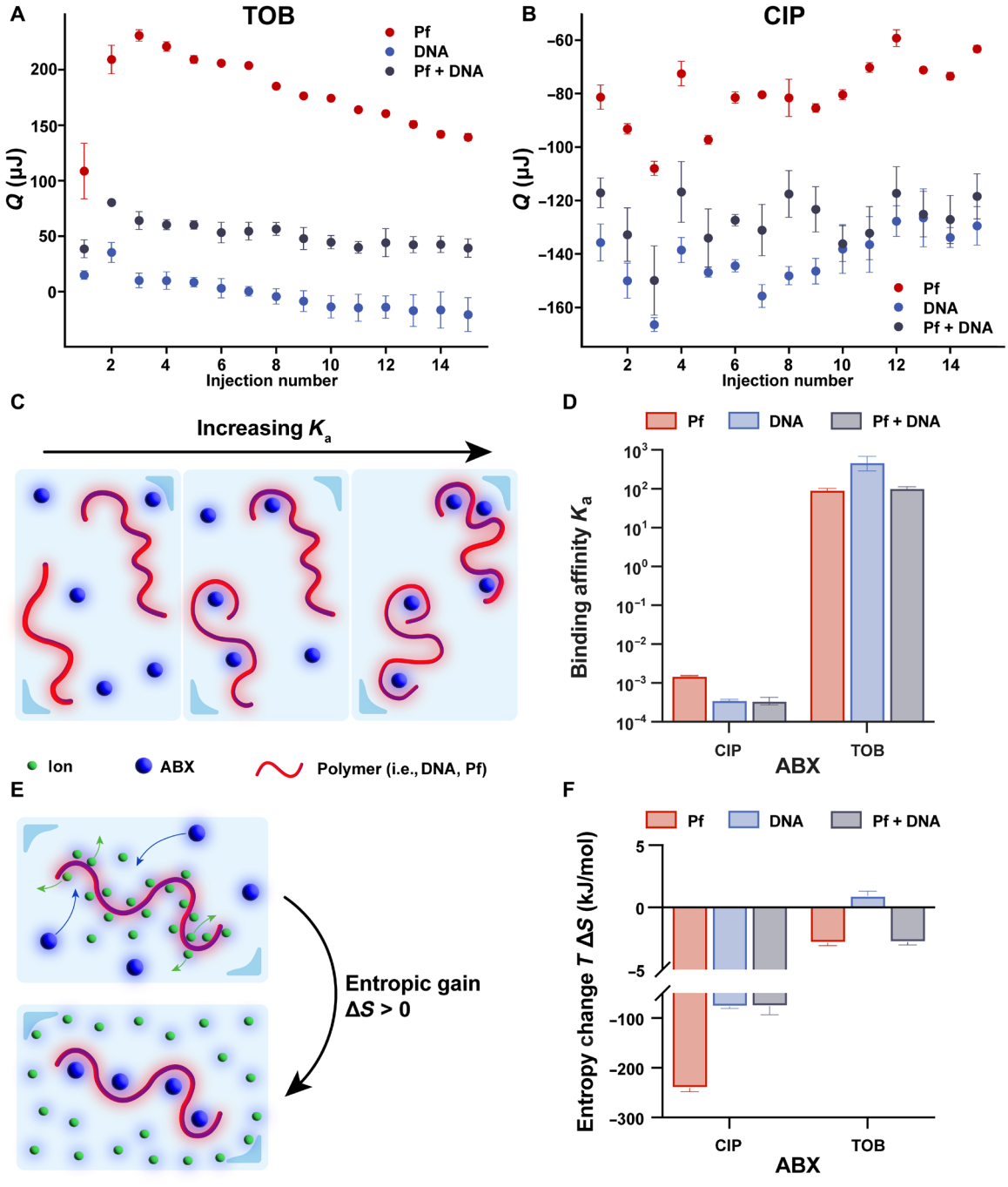

Fig. 3. ITC reveals that the electrostatic interaction is antibiotic specific. (**A**) Heat per injection corrected for blank conditions for three conditions: TOB in DNA (4 mg/ml; $n = 3$), TOB in Pf4 [10^{11} plaque-forming units (PFU)/ml; $n = 3$], and TOB in DNA (4 mg/ml) and Pf4 (10^{11} PFU/ml; $n = 3$). (**B**) Heat released per injection corrected for blank conditions for three conditions: CIP in DNA (4 mg/ml; $n = 3$), CIP in Pf4 (10^{11} PFU/ml; $n = 3$), and CIP in DNA (4 mg/ml) and Pf4 (10^{11} PFU/ml; $n = 3$). (**C**) A larger binding affinity, K_a, indicates more antibiotics and polymers bound together at equilibrium. (**D**) Binding affinities for the positively charged antibiotic, TOB, and neutrally charged antibiotic, CIP, in Pf phage (TOB, $n = 2$; CIP, $n = 2$), DNA (TOB, $n = 3$; CIP, $n = 2$) and both Pf phage and DNA (TOB, $n = 2$; CIP, $n = 3$) are shown. Error bars show ±1 SD. (**E**) Larger and more positively charged antibiotics displacing positive counter ions surrounding negatively charged polymers such as DNA and Pf phage can lead to a positive change in entropy. (**F**) Entropic change is positive for the positively charged antibiotic, TOB, and negative for the neutral antibiotic, CIP. The reference concentration to determine entropy change was 0.003 M.

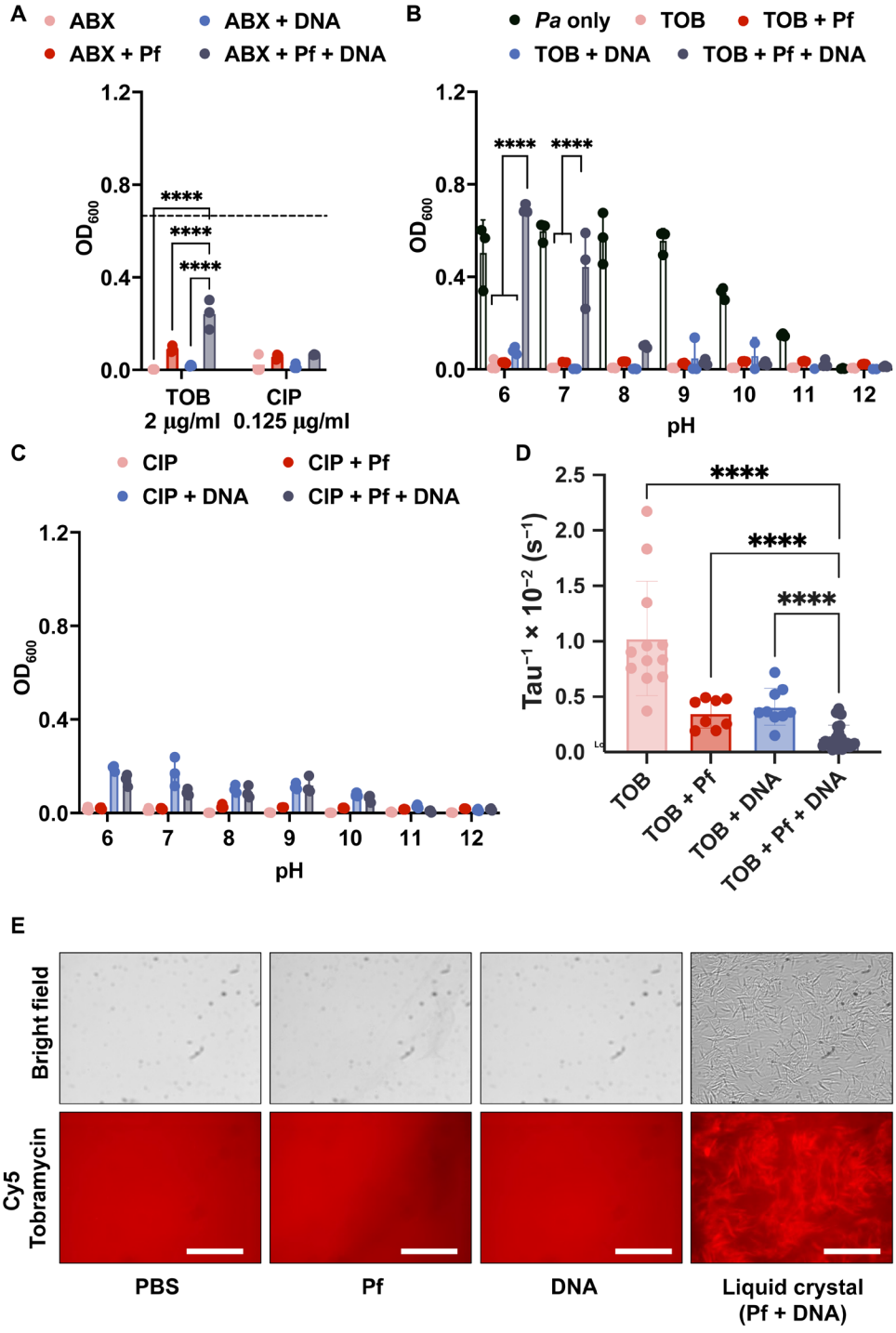

Fig. 4. Sputum polymers mixed with Pf phage reduce efficacy and diffusion of antibiotics in a charge-dependent manner. (**A**) Pf and DNA affect TOB and COL efficacy against *Pa*. Dashed line indicates the OD for *Pa* alone ($n = 3$). Phages and DNA affect (**B**) TOB, but not (**C**) CIP, antimicrobial activity in a pH-dependent manner against PA14 ($n = 3$). (**D**) The effective diffusion rate, tau^{-1}, was found from the FRAP recovery curves of Cy5-TOB in PBS ($n = 12$), Pf ($n = 9$), DNA ($n = 12$), and both Pf and DNA ($n = 13$). (**E**) The binding of Cy5-TOB to Pf phage–mediated liquid crystals (DNA + Pf condition) was visualized by fluorescent microscopy. ****$P \leq 0.0001$, two-way ANOVA for OD_{600} and unpaired *t* test for tau^{-1} plots. Scale bar, 20 um.

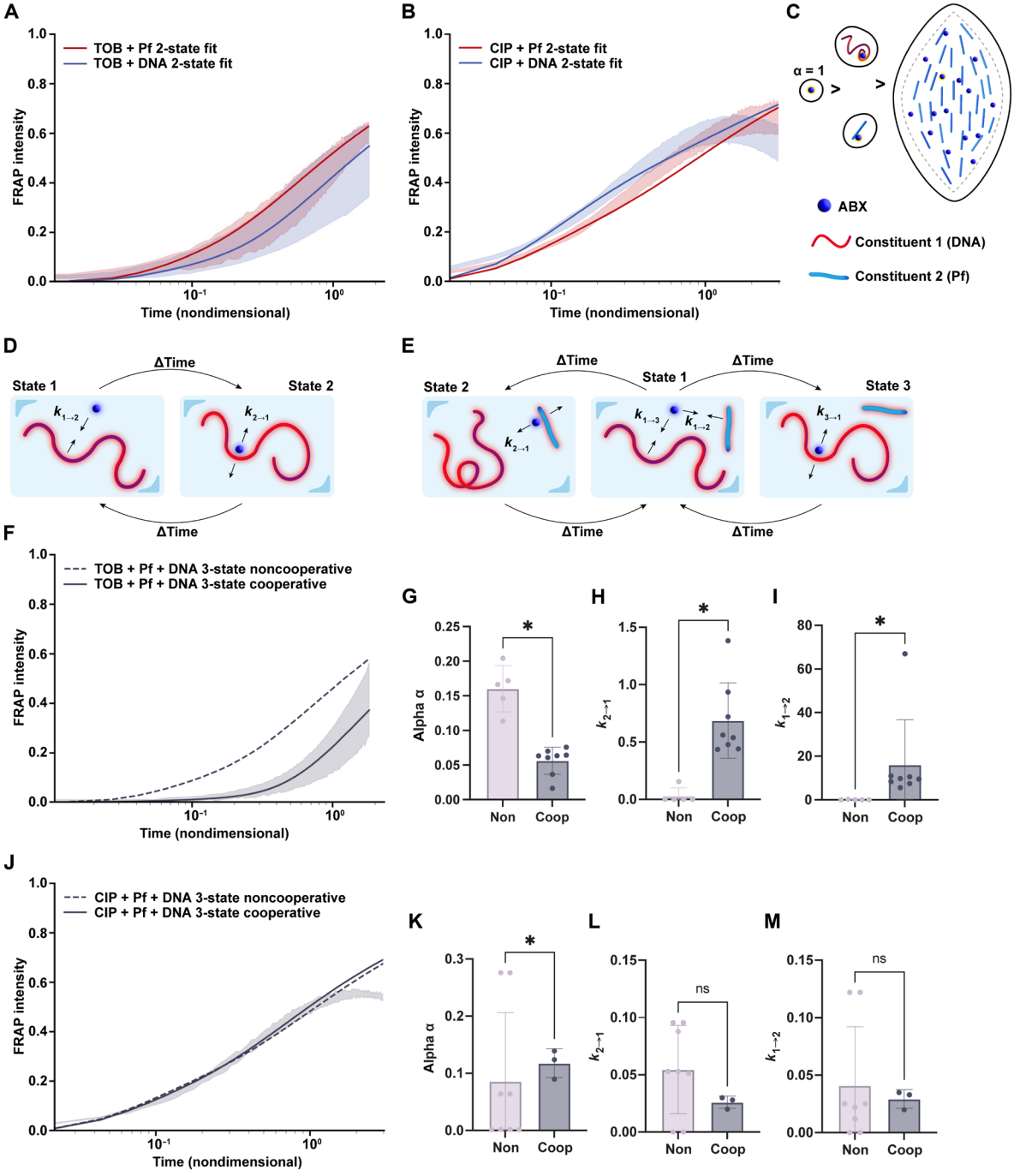

Fig. 5. A set of two-state and three-state models demonstrates that liquid crystals reduce the diffusion of charged antibiotics through electrostatic interaction. The distribution over 1 SD of the FRAP recovery data is shown along with the best fit of the two-state model to each condition for (**A**) Cy5-TOB and (**B**) Cy5-CIP in either Pf phages or DNA. (**C**) Schematics demonstrate that electrostatic binding could affect the diffusion of positively charged antibiotics, such as TOB, by increasing the size of the diffusing mass. (**D**) The FRAP data were modeled using a newly derived diffusion model that accounts for electrostatic attraction between the antibiotic and another constituent (two-state model). (**E**) The FRAP data were modeled using a newly derived diffusion model that accounts for electrostatic attraction between the antibiotic and two other constituents, attributing different diffusion times to each type of bound state: antibiotic bound to Pf phages, antibiotic unbound to anything, and antibiotic bound to DNA. The distribution over 1 SD of the FRAP recovery data is shown along with the noncooperative and cooperative three-state models to each condition for (**F**) Cy5-TOB and (**J**) Cy5-CIP in mixtures of Pf phages and DNA. The noncooperative FRAP recovery assumes no additional contribution to diffusion due to liquid crystal (dashed), while the cooperative FRAP recovery shows the effect of liquid crystal formation on antibiotic diffusion (solid). The change in the diffusion and binding parameters found via the model for (**G** to **I**) TOB or (**K** to **M**) CIP bound to Pf phages or antibiotic bound to a liquid crystal structure of Pf phages and DNA are shown. [(G) to (I)] The values for TOB show statistically different values demonstrating an additional diffusion hindrance from the liquid crystal. Alpha is the change in relative diffusion compared to antibiotic alone in a buffer solution, where a lower alpha value corresponds to a slower diffusion. $k_{2\to1}$ and $k_{1\to2}$ are unbinding and binding rate constants, respectively, where the ratio of the two gives the equilibrium constant of the binding interaction. A higher equilibrium constant implies a longer time spent bound. *$P \leq 0.05$.

this noncooperative three-state model. We found that the resulting noncooperative three-state model predicted a faster recovery in TOB fluorescence than the experimental data shown (Fig. 5F). On the other hand, the fluorescent recovery of CIP in DNA and Pf phages was almost perfectly predicted by the noncooperative three-state model (Fig. 5J). Given previous findings of liquid crystal formation between Pf phages and DNA, we decided to quantify the effect of liquid crystals on diffusion under these conditions. To do so, we used the same three-state model, but this time, we only used the parameters for DNA obtained from the two-state model fit of the FRAP data for antibiotics in DNA. The parameters for the second constituent to which the antibiotics can bind were fit to the FRAP data for a mixture of DNA and Pf phages. By fitting the parameters of the second constituent to the FRAP data, we imply that there is cooperativity between antibiotic binding to DNA and binding to Pf. Thus, these new parameters for the second constituent reflected any additional hindrance to antibiotic diffusion from DNA and Pf phage interactions, which stem from liquid crystal formation. For TOB, the diffusion rate α of the second constituent was lower than the α in the noncooperative three-state model (Fig. 5G). In contrast, the diffusion rate for CIP remained, on average, the same between the noncooperative and cooperative models (Fig. 5K). The kinetic parameters $k_{1\rightarrow2}$ and $k_{2\rightarrow1}$ for TOB suggested faster binding to the liquid crystal and more time spent bound to the liquid crystal than when TOB was in a solution of just Pf phages (Fig. 5, H and I). The kinetic parameters for CIP were similar between the cases of Pf phages only (noncooperative) and Pf + DNA liquid crystals (cooperative) (Fig. 5, L and M). Overall, we found that for TOB, not only was the diffusion in Pf phage and DNA slower than when we assumed noncooperativity but cooperativity also appeared to increase the rate of binding of TOB to the second constituent (Fig. 5, G to I).

To further validate the effect of the liquid crystal on TOB diffusion, we compared the FRAP data for TOB in DNA and Pf phages to data for TOB with DNA and a nonliquid crystal–forming bacteriophage, LPS-5 (fig. S14). Combining DNA and LPS-5 did not significantly change the FRAP recovery compared to TOB diffusion in DNA alone (fig. S14, A and B). Using the same three-state FRAP models above, we found that the predicted FRAP recovery with the three-state noncooperative model aligned with the FRAP recovery curve for TOB in a mixture of DNA and LPS-5 (fig. S14, A and B). Furthermore, we fitted the three-state noncooperative model to the FRAP recovery data for the condition of DNA and LPS-5. We found no significant difference in the parameters between the cooperative and noncooperative models (fig. S14C). The main difference between LPS-5, a lytic phage that infects *Pa*, and Pf phage is the formation of liquid crystals between Pf and DNA, so the results suggest that liquid crystals significantly affect TOB transport.

DISCUSSION

In this study, we have asked how Pf phages and polymers present in sputum prevent the diffusion of TOB, an inhaled antibiotic commonly used to treat chronic *Pa* infection in pwCF. We demonstrated that the diffusion of TOB, a positively charged antibiotic, through networks of Pf and sputum polymers, is limited by electrostatic interactions. Conversely, CIP, a neutrally charged antibiotic, exhibits limited electrostatic attraction with Pf or sputum components. Moreover, higher-order, crystalline structures formed between Pf phages and sputum polymers further slow the diffusion of TOB due to these charge-based interactions (Fig. 6). These results are consistent with previously published studies, showing that positively charged antibiotics have reduced antimicrobial activity when Pf is present (*26*, *31*) and establish a biophysical explanation for these interactions.

The data presented here generally agree with previous modeling studies. Rossem *et al.* (*33*, *34*) modeled antibiotic diffusion in liquid crystal tactoids formed by Pf phages and sputum biopolymers. Their mathematic model yields results for antibiotic diffusion that agree broadly with the experimentally observed results. Their model was constrained to the tactoid volume, but in real sputum environments, most of the volume is unlikely to consist of liquid crystals. The focus on the tactoid space could explain Rossem *et al.*'s (*33*, *34*) own observation that the timescales predicted by their model are not sufficiently long to explain antibiotic tolerance on the order of hours. Likely in the sputum environment, liquid crystal tactoids form spontaneously because of local density changes in biopolymers and Pf phages so that the sputum environment contains regions of tactoids and regions devoid of tactoids. Our focus when modeling antibiotic diffusion was on handling the temporal heterogeneity observed through the binding and unbinding of the sputum environment and not just the tactoid volume. The larger scope of our model sacrifices spatial resolution, which is captured explicitly in Rossem *et al.*'s approach *(33, 34)*. Thus, a comprehensive model of antibiotic interaction with *Pa* in the sputum environment in the presence of Pf would incorporate aspects of both our model and that of Rossem *et al. (33, 34)*.

Our own models reveal cooperativity between the binding of TOB to Pf phages and DNA but not between the binding of CIP to Pf phages and DNA. Despite the fact that the pH measurement and how pH affects antimicrobial in CF airways have been inconclusive, several studies have suggested that the average pH in sputum and airway is 6.6 to 7 (*42*, *43*), which is the condition that TOB carries positive charges. If the binding between TOB and sputum components was the only factors hindering its diffusion, we would not have observed this cooperativity. Thus, cooperativity arises from the additional influence of liquid crystals that form at the DNA and Pf phage concentrations used in our experiments (Fig. 6) (*26*). The set of models developed in this paper provides powerful tools for analyzing diffusion with binding due to how the parameters can be translated across the three different models. The simplicity behind these models makes them easily applicable to a wide range of scenarios where one would want to capture the main contributing factor influencing observed diffusion trends.

Further modeling studies need to be performed to better understand whether the structure of the polymer or charge of the polymer plays a larger role in hindering antibiotic diffusion in liquid crystals and whether the results we observed for DNA can be extended to other negatively charged biopolymers found in the sputum and *Pa* biofilms. For example, mucin is a large component of the secretory apparatus in the airways, so any interactions between mucin and Pf would be valuable for therapeutic purposes. In this study, we focused on DNA due to its markedly increased presence during *Pa* infection compared to other polymers such as mucin. Our data show that Pf with simple sputum (containing mucin) correlates to reduced antibiotic diffusion (Fig. 2); however, it necessitates the study of Pf and mucin interaction as a next step. Similarly, we confined our study to TOB and CIP. Aerosolized AZT is also available for chronic *Pa* infection in pwCF in the United States and was found to exhibit slightly less efficacy in the presence of mucin, DNA, and Pf (fig. S4A). We also found that COL, another commonly prescribed antibiotic, appeared to exhibit similar trends in activity due to Pf presence as TOB (fig. S4). We

hypothesize, however, that these molecules have a different mechanism of interaction with Pf phage and sputum polymers than TOB and CIP due to factors such as a larger size (COL) or a positively charged nature (AZT) (table S2). It would be therefore important to perform further investigations for these other antibiotics in the future.

Electrostatic binding between Pf phage and positively charged antibiotics could be attenuated as a strategy for addressing antibiotic diffusion hindrance. For example, positively charged antimicrobial peptides, such as LL-37, have been shown to interact with negatively charged cellular components (*44*), such as lipopolysaccharides (*45*), eDNA (*46*), and double-stranded RNA (*47*). This molecule and other similarly charged molecules could compete with positively charged antibiotics in binding to Pf phage and sputum biopolymers. By replacing the antibiotics in the bound state, more antibiotics can freely diffuse, thus potentially increasing antibiotic efficacy.

One limitation of this work is the simplified model system we used because it lacks some of the complexities of sputum produced in the CF airway. We nonetheless believe that our models capture some of the relevant biophysical attributes of this system. It has previously been shown that high–molecular weight DNA with Pf phages alone can lead to the formation of liquid crystal tactoids (*26*). Studies have suggested that DNA is an important structural component in biofilms and is negatively associated with pulmonary function and disease severity in pwCF (*48*–*50*). Therefore, we simplified our model system to just Pf phage and DNA. Future studies will examine antibiotic and Pf phage interactions in more complex sputum formulations.

In summary, our analysis suggests that Pf phages in sputum reduce the diffusion of charged antibiotics due to a greater binding constant. In the future, we will leverage this understanding of the interaction between positively charged antibiotics and Pf phages to design or find molecules that recover the diffusion of and rescue the antimicrobial activities of positively charged antibiotics against the clinically significant *Pa*.

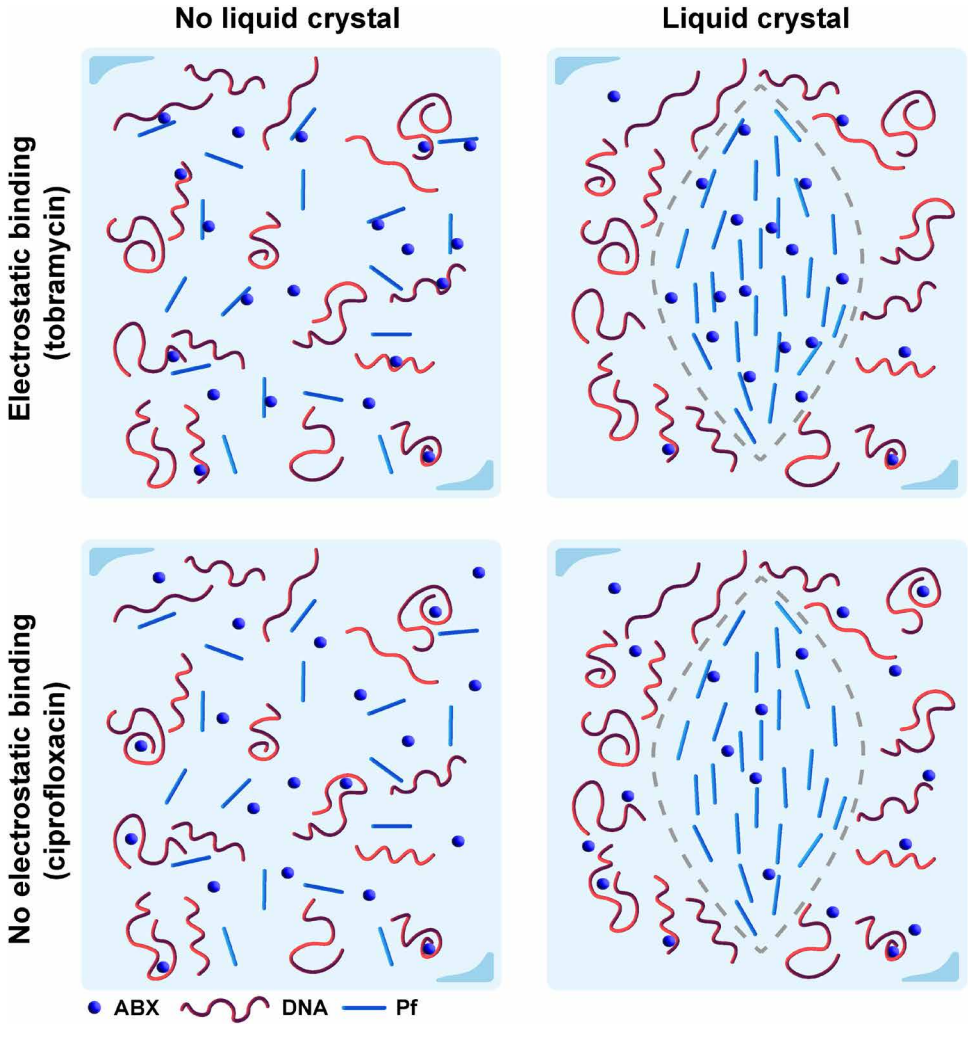

Fig. 6. Depiction of the interaction mechanism among positively charged and neutral antibiotics with the sputum components Pf phages and DNA. For positively charged antibiotics such as TOB, the lack of a liquid crystal formation hinders diffusion through binding with sputum components Pf phages and DNA (top left). When there is liquid crystal formation, these antibiotics are further sequestered and experience increased rate of binding due to the higher density of polymers in the liquid crystal tactoid (top right). For neutral antibiotics such as CIP, the lack of electrostatic attraction results in little influence of sputum polymers on diffusion, although in the liquid crystal, the higher density of polymers will decrease effective diffusion (bottom row).

MATERIALS AND METHODS

Collection of CF sputum

Sputum samples from patients with CF were collected by spontaneous expectoration during clinic visits or hospitalizations. Patients and healthy controls were consented for sputum collection under Institutional Review Board approved protocols #37232, 56996, or 11197. Sputum was aliquoted and frozen at −80°C before use.

Bacterial culture

PA14 was streaked from a frozen glycerol stock onto LB agar (BD BBL) plates and incubated overnight at 37°C with 5% carbon dioxide (CO_2) until individual colonies formed. A single colony was inoculated into 3 ml of LB media and grown at 37°C in a shaking incubator at 250 rpm to an optical density at 650 nm (OD_{650}) of 0.4, corresponding to ~5×10^8 colony-forming units (CFU)/ml. Bacterium cultures were adjusted to 1×10^6 CFU/ml to prepare a working stock for all experiments.

Bacteriophage isolation and propagation

Phages were propagated on the basis of the previously described protocol (*51*). Briefly, planktonic bacterial cultures were grown to an OD_{650} of 0.4, then infected with phage stock, and further grown for 2 hours. Then, 150 ml of LB media were inoculated with phage-infected bacterial cultures and incubated at 37°C overnight shaking. The overnight cultures were centrifuged (8000*g* for 30 min at 4°C) and filtered through a 0.22-μm polyethersulfone membrane (Corning, New York, product #4311188) to remove bacterial debris. The filtrate was treated with benzonase nuclease (5 U/ml; Sigma-Aldrich, Saint Louis, MO, catalog no. E8263) at 37°C. After benzonase treatment, filtrates were centrifuged (8000*g* at 4°C) overnight, and the pellet was resuspended and quantified for titer by plaque assay.

In vitro antimicrobial activity

Four antibiotics were used in this experiment, including TOB, CIP, COL, and AZT. Each antibiotic was dissolved in sterile distilled water to make stock solutions with concentrations of 1 mg/ml and diluted to indicated concentration in LB. Salmon sperm DNA (Sigma-Aldrich, Saint Louis, MO, product #D1626) and mucin (Sigma-Aldrich, Saint Louis, MO, product #M1778) were dissolved in LB. The bacterial killing by different antibiotics in various conditions was determined according to the standard Clinical and Laboratory Standards Institute broth-microdilution method and adapted from previous studies (*37*). Briefly, a 100-μl aliquot of a bacterial suspension was added to each well ($n = 3$) containing 100 μl of solutions that contained antibiotics only, antibiotics with Pf phages, antibiotics with DNA or DNA and mucin, or antibiotics with Pf with DNA or DNA and mucin in a 96-well plate to achieve 5×10^5 CFU per well. The final concentrations of Pf phages, DNA, and mucin are 10^{11} plaque-forming units (PFU)/ml, 4 mg/ml, and 8% solids, respectively. The 96-well plate was incubated at 37°C for 18 to 24 hours under static conditions. The OD_{600} was measured in a Biotek Synergy HT (BioTek, Winooski, VT, USA), where higher OD_{600} indicated less bacterial death.

ITC studies

The thermal behavior of antibiotics interaction with Pf phages and polymers was studied using the ITC instrument (TA Instruments Nano ITC). Antibiotics were titrated from the syringe into the sample cell that contains PBS only, Pf4 phages (10^{11} PFU/ml) in PBS, or Pf4 (10^{11} PFU/ml) and DNA (1 mg/ml) in PBS. After each injection, the heat exchange produced from the interaction was measured by ITC calorimeter. Between each injection, the system was allowed to attain equilibrium.

For an experiment titrating component 1 (i.e., antibiotic) into component 2 (i.e., DNA), data were obtained from for the (i) titration of component 1 into component 2, (ii) titration of component 1 into a buffer solution without component 2, and (iii) titration of a buffer solution without component 1 into component 2. The last two titrations are considered blanks for the first titration and are subtracted from the first titration to correct for entropic change due to volume change. These corrected heat change data were fit using a nonlinear least-squares regression to a two-component thermodynamic binding model. The binding model contains two contributions: one from ion pairing ("IP"), or electrostatic binding, and one from phase change ("c"), possibly precipitation or liquid crystallization (*39*).

$$Q_{\text{bind}}(i) = nM_t\,(i)\,V_0\Delta H_{IP}\Theta + n_cM_t\,(i)\,V_0\Delta H_c\Theta_c\,(i)$$

For antibiotic binding to a polymer, there are multiple binding sites per polymer chain. Each binding event of an antibiotic molecule to the polymer is assumed to be independent of other binding events along the same polymer.

$$\Theta(i) = \frac{K_aX_t\,(i)}{1 + K_aX_t\,(i)}$$

The fitted binding affinity, K_a, was directly compared across the conditions. The entropy change, ΔS, was found by the following thermodynamic relation using a reference concentration of 0.003 M, which is about the concentration of CIP used in its ITC measurements. In this equation, ΔH_{IP} and K_a are found through fitting the data to the model, and R and T, the gas constant and the temperature, are known quantities.

$$\Delta S = \frac{\Delta H_{IP}}{T} + R\text{In}\,(K_aX_{\text{ref}})$$

Measurements of diffusion of fluorescently tagged antibiotics by FRAP

Cy5-labeled antibiotics (TOB and CIP) purchased from Biosynthesis Inc. were used in the experiment. Six conditions were used to investigate the diffusion of antibiotics, including control, Pf4 phages only, polymers only, and Pf4 mixed with polymers. Each condition was added with 1 μl of fluorescent antibiotic with a concentration of 1 mg/ml. FRAP experiments were performed using a Leica DMI 8 confocal microscope with a 10× dry objective. In each FRAP experiment, a prebleach image was acquired at 2% of the maximum laser intensity. Then, the mixture was bleached for 30 s at the maximum laser intensity and recorded intensity recovery for 3 min.

Methods for FRAP analysis

A Green's function was used to denote the distribution of trajectories of the fluorescent molecules in a 1D system and combined with systems of differential equations accounting for the kinetics of binding events to model the fluorescent recovery when binding affects diffusion. We assume no photofading. The three models presented here, one-state, two-state, and three-state models, allow hypothesis testing of any type of binding interactions that could be occurring in a FRAP experiment and allow extraction of more information from a single FRAP measurement.

One-state FRAP model: Diffusion only

One-state model assumes that fluorescent particles move with diffusion coefficient D with no kinetic events or binding occurring. A 1D line of length L is imagined, with the position $x = 0$ at the center such that from $x = 0$ to the edge of the line is a distance $L/2$ (fig. S15). It is assumed that the probability that a particle starting at a position x_0 ends up at a position x at time t follows a normal distribution.

$$G(x \mid x_0; t) = N\exp\left[-\frac{(x-x_0)^2}{4Dt}\right]$$

In this system, numerous fluorescent particles are in the area, but the fluorescence at position $x = 0$ is measured as the signal. The signal at position $x = 0$ is found by integrating over all possible starting particles at positions $x_0 = 0.1L, 0.2L, 0.3L\ldots$ that will be at position $x = 0$ at time t.

$$\mathrm{FRAP}(t) = 2\int_{L/2}^{\infty} dx_0 G(0 \mid x_0; t)$$

After replacing the probability distribution in the above equation with the normal distribution function, the fluorescent intensity as a function of time for an area of interest with size L is found.

$$\mathrm{FRAP}(t) = 1 - erf\left(\frac{L}{4\sqrt{Dt}}\right)$$

Furthermore, this model can be nondimensionalized with nondimensionalization factor D/L^2.

$$\mathrm{FRAP}(\tau) = 1 - erf\left(\frac{1}{4\sqrt{\tau}}\right)$$

Two-state FRAP model: Diffusion and binding to one constituent

The second model, two-state model, assumes that in addition to the diffusion of the fluorescent particle at some diffusion coefficient $D_1 = D$ ("state 1"), these particles can bind to some other constituent that has a diffusion coefficient of $D_2 = \alpha D$ ("state 2"), where $\alpha < 1$ (i.e., being bound to this other constituent slows down the particle's diffusion compared to when it is free). The binding process is transient, with a rate of binding to the other constituent $k_{1\to2}$ and unbinding from the other constituent $k_{2\to1}$ (Fig. 5D). The following reaction and defined kinetic parameters describe this two-state scenario.

$$\mathrm{State1} \underset{k_{2\to1}}{\overset{k_{1\to2}}{\rightleftarrows}} \mathrm{State2}$$

Note that from here on, the use of the variable t corresponds to nondimensionalized time, which is denoted in the one-state model derivation with the letter τ.

A Green's function is used to denote the spatial integration of the fluorescence as in the one-state model. It is assumed an initial condition for the fluorescent signal

$$G_1(x, t=0) = \delta(x)p_1$$
$$G_2(x, t=0) = \delta(x)p_2$$

where

$$p_1 = \frac{k_{2\to1}}{k_{2\to1}+k_{1\to2}}$$
$$p_2 = \frac{k_{1\to2}}{k_{2\to1}+k_{1\to2}}$$

With two states, this model requires a set of differential equations to describe the diffusion and kinetics of the system.

$$\frac{\partial G_1}{\partial t} = D_1\frac{\partial^2 G_1}{\partial x^2} + k_{2\to1}G_2 - k_{1\to2}G_1$$
$$\frac{\partial G_2}{\partial t} = D_2\frac{\partial^2 G_2}{\partial x^2} + k_{2\to1}G_2 - k_{1\to2}G_1$$

Solving this set of equations involves Laplace ($t \to s$) and Fourier ($x \to k$) transforms to make the operation algebraic. The Green's functions for state A and state B, which represent the fluorescent contributions from each state to the overall average fluorescent intensity, are solved for and summed to get the total of the fluorescent signal because the total fluorescence comes from free particles in solution and particles bound to polymers. Both states contribute to the total fluorescence but will simply have different rates of fluorescent fluctuation given the differences in diffusion. Last, the transform is inverted to give the fluorescent signal as a function of time.

The two-state model was evaluated using diffusion rates for the two states that are equal and found to agree with the one-state model using that same diffusion rate, which is as expected (fig. S16A). When state 2 is given a slower diffusion rate and the rate of unbinding is lowered, the two-state model predicts a slower recovery before eventually returning to the same full fluorescent recovery as the one-state model (fig. S16B). The emergence of the second plateau in fluorescence intensity recovery is much more likely to occur when the relative diffusion rate α is low (fig. S17A). Furthermore, analysis of two scenarios, low α and the upper limit of α, shows that only in the limit of the relative diffusion between the two states being different does there emerge any dependence of the fluorescence intensity recovery on the rates of binding (fig. S17, B to E).

Three-state FRAP model: Diffusion and binding to two kinetically distinct entities

In this scenario, there are two different entities that the particle can bind to, and those two entities also have different, distinct diffusion rates (Fig. 5E). State 1 is still the free particle state. State 2 is when the particle is bound to the first constituent and has diffusion $D_2 = \alpha_2 D$. "State 3" is when the particle is bound to the second constituent and has diffusion $D_3 = \alpha_3 D$. In both cases, the diffusion of the bound state is lower than that of the free particle, denoted as $D_1 = D$ (i.e., α_2 and $\alpha_3 < 1$).

$$\mathrm{State2} \underset{k_{1\to2}}{\overset{k_{2\to1}}{\rightleftarrows}} \mathrm{State1} \underset{k_{3\to2}}{\overset{k_{1\to3}}{\rightleftarrows}} \mathrm{State3}$$

The binding and unbinding of the particle to each constituent are governed the respective on and off rates. Similarly to the two-state model, a set of differential equations governs the diffusion and kinetics of this system with initial conditions for the Green's functions.

$$\frac{\partial G_1}{\partial t} = D_1 \frac{\partial^2 G_1}{\partial x^2} - (k_{1\to2} + k_{1\to3})G_1 + k_{2\to1}G_2 + k_{3\to1}G_3$$
$$\frac{\partial G_2}{\partial t} = D_2 \frac{\partial^2 G_2}{\partial x^2} - k_{2\to1}G_2 + k_{1\to2}G_1$$
$$\frac{\partial G_3}{\partial t} = D_3 \frac{\partial^2 G_3}{\partial x^2} - k_{3\to1}G_3 + k_{1\to3}G_1$$

Initial conditions are similar to the two-state model.

$$G_1(x, t=0) = \delta(x)p_1$$
$$G_2(x, t=0) = \delta(x)p_2$$
$$G_3(x, t=0) = \delta(x)p_3$$

where

$$p_1 = \frac{k_{2\to1} + k_{3\to1}}{k_{2\to1} + k_{3\to1} + k_{1\to2} + k_{1\to3}}$$
$$p_2 = \frac{k_{1\to2}}{k_{2\to1} + k_{3\to1} + k_{1\to2} + k_{1\to3}}$$
$$p_3 = \frac{k_{1\to3}}{k_{2\to1} + k_{3\to1} + k_{1\to2} + k_{1\to3}}$$

Solving the set of differential equations involves Laplace and Fourier transformations to obtain the individual Green's functions for each state. The inversion of the Laplace transform to the time domain gives the fluorescent recovery over time.

The three-state model was evaluated using diffusion rates for the two bound states that are equal to the free state and found to agree with the one-state model and two-state model in the limit of equal diffusion rates, which is as expected (fig. S18A). When we slow the diffusion of states 1 and 2, the three-state model predicts a slower recovery and exhibits a delay in the recovery from even the two-state model, which has the same diffusion rate as one of the states in the three-state model. Thus, the three-state model can account for the additional slowdown of the fluorescent particle when it is bound to an even slower additional constituent (fig. S18B).

When one relative diffusion rate α is high, almost no scenario has a large effect on the fluorescence recovery curve except when the binding rates for the state with the high diffusion is low and the other state has low diffusion and fast binding rates (fig. S19B). Else, there is little effect on the fluorescence recovery (fig. S19, D, F, and H). In the limit of low α, there is almost always a dependence on the recovery plateaus observed as a function of the other relative diffusion rate and binding rates (fig. S19, A, E, and G). The one exception is if the binding rate of the state with the low relative diffusion rate is much higher than the other state ($k_{on}2$, $k_{off}2 > k_{on}1$, $k_{off}1$ for low α2). In this case, there is little effect of varying the diffusion rate of the other state α1 (fig. S19C).

Fitting the FRAP models to the FRAP data

FRAP recovery curves were fit to the FRAP models using nonlinear least-squares regression. FRAP data for antibiotics diffusing in buffer, where there is assumed to be no binding occurring, were fit to the one-state model. The nondimensionalization factor from this fit was used to nondimensionalize the time for all other conditions that were fit to the two- and three-state models. FRAP data for antibiotics in DNA or Pf phage (only one other constituent present) were fit to the two-state model after nondimensionalizing time. The parameters found for DNA or Pf phage in the two-state model were plugged into the three-state model (assumes binding to be occurring independently or noncooperatively to DNA or Pf phage) to generate the predicted FRAP recovery curves for antibiotics in DNA and Pf phage. Last, the DNA parameters found from fitting antibiotics in DNA to the two-state model were kept constant, and the binding parameters for constituent 2 in the three-state model were optimized to find the best fit to the antibiotics in DNA and Pf phage FRAP recovery curves ("cooperative three-state"). Numerical evaluation of each model was done in a Python Jupyter Notebook, which is available by email request.

Statistics

All column graphs and statistical analyses were performed using GraphPad Prism version 9 software. Outlier analysis was performed using the robust regression and outlier removal method with no more than 1% of identified outliers to be false. For the bacterial killing assay, statistical significance was assessed by two-way analysis of variance (ANOVA) with Tukey's multiple comparisons tests.

Supplementary Materials

This PDF file includes:

Figs. S1 to S19
Tables S1 and S2

REFERENCES AND NOTES

1. J. B. Lyczak, C. L. Cannon, G. B. Pier, Lung infections associated with cystic fibrosis. *Clin. Microbiol. Rev.* **15**, 194–222 (2002).
2. Cystic Fibrosis Foundation, Cystic Fibrosis Foundation patient registry 2021 annual data report (2022).
3. J. K. Harris, B. D. Wagner, E. T. Zemanick, C. E. Robertson, M. J. Stevens, S. L. Heltshe, S. M. Rowe, S. D. Sagel, Changes in airway microbiome and inflammation with ivacaftor treatment in patients with cystic fibrosis and the G551D mutation. *Ann. Am. Thorac. Soc.* **17**, 212–220 (2020).
4. M. Rosenfeld, R. L. Gibson, S. McNamara, J. Emerson, J. L. Burns, R. Castile, P. Hiatt, K. McCoy, C. B. Wilson, A. Inglis, A. Smith, T. R. Martin, B. W. Ramsey, Early pulmonary infection, inflammation, and clinical outcomes in infants with cystic fibrosis. *Pediatr. Pulmonol.* **32**, 356–366 (2001).
5. M. W. Konstan, W. J. Morgan, S. M. Butler, D. J. Pasta, M. L. Craib, S. J. Silva, D. C. Stokes, M. E. Wohl, J. S. Wagener, W. E. Regelmann, C. A. Johnson, Coordinators of the epidemiologic study of cystic, risk factors for rate of decline in forced expiratory volume in one second in children and adolescents with cystic fibrosis. *J. Pediatr.* **151**, 134–139.e1 (2007).
6. G. M. Nixon, D. S. Armstrong, R. Carzino, J. B. Carlin, A. Olinsky, C. F. Robertson, K. Grimwood, Clinical outcome after early *Pseudomonas aeruginosa* infection in cystic fibrosis. *J. Pediatr.* **138**, 699–704 (2001).
7. J. Emerson, S. McNamara, A. M. Buccat, K. Worrell, J. L. Burns, Changes in cystic fibrosis sputum microbiology in the United States between 1995 and 2008. *Pediatr. Pulmonol.* **45**, 363–370 (2010).
8. P. J. Mogayzel Jr., E. T. Naureckas, K. A. Robinson, C. Brady, M. Guill, T. Lahiri, L. Lubsch, J. Matsui, C. M. Oermann, F. Ratjen, M. Rosenfeld, R. H. Simon, L. Hazle, K. Sabadosa, B. C. Marshall, C. Cystic, Cystic Fibrosis Foundation pulmonary guideline. Pharmacologic approaches to prevention and eradication of initial *Pseudomonas aeruginosa* infection. *Ann. Am. Thorac. Soc.* **11**, 1640–1650 (2014).
9. G. Doring, P. Flume, H. Heijerman, J. S. Elborn; Consensus Study Group, Treatment of lung infection in patients with cystic fibrosis: Current and future strategies. *J. Cyst. Fibros.* **11**, 461–479 (2012).
10. D. P. Nichols, S. J. Morgan, M. Skalland, A. T. Vo, J. M. Van Dalfsen, S. B. Singh, W. Ni, L. R. Hoffman, K. McGeer, S. L. Heltshe, J. P. Clancy, S. M. Rowe, P. Jorth, P. K. Singh; PROMISE-Micro Study Group, Pharmacologic improvement of CFTR function rapidly decreases sputum pathogen density, but lung infections generally persist. *J. Clin. Invest.* **133**, e167957 (2023).
11. P. J. Mogayzel Jr., E. T. Naureckas, K. A. Robinson, G. Mueller, D. Hadjiliadis, J. B. Hoag, L. Lubsch, L. Hazle, K. Sabadosa, B. Marshall, C., Cystic fibrosis pulmonary guidelines. *Am. J. Respir. Crit. Care Med.* **187**, 680–689 (2013).
12. M. N. Hurley, A. H. Ariff, C. Bertenshaw, J. Bhatt, A. R. Smyth, Results of antibiotic susceptibility testing do not influence clinical outcome in children with cystic fibrosis. *J. Cyst. Fibros.* **11**, 288–292 (2012).

13. R. Somayaji, M. D. Parkins, A. Shah, S. L. Martiniano, M. M. Tunney, J. S. Kahle, V. J. Waters, J. S. Elborn, S. C. Bell, P. A. Flume, D. R. VanDevanter, Antimicrobial susceptibility testing (AST) and associated clinical outcomes in individuals with cystic fibrosis: A systematic review. *J. Cyst. Fibros.* **18**, 236–243 (2019).
14. J. D. Cogen, K. B. Whitlock, R. L. Gibson, L. R. Hoffman, D. R. VanDevanter, The use of antimicrobial susceptibility testing in pediatric cystic fibrosis pulmonary exacerbations. *J. Cyst. Fibros.* **18**, 851–856 (2019).
15. A. Mai-Prochnow, J. G. Hui, S. Kjelleberg, J. Rakonjac, D. McDougald, S. A. Rice, Big things in small packages: The genetics of filamentous phage and effects on fitness of their host. *FEMS Microbiol. Rev.* **39**, 465–487 (2015).
16. J. Rakonjac, N. J. Bennett, J. Spagnuolo, D. Gagic, M. Russel, Filamentous bacteriophage: Biology, phage display and nanotechnology applications. *Curr. Issues Mol. Biol.* **13**, 51–76 (2011).
17. P. Knezevic, M. Voet, R. Lavigne, Prevalence of Pf1-like (pro)phage genetic elements among *Pseudomonas aeruginosa* isolates. *Virology* **483**, 64–71 (2015).
18. K. Fiedoruk, M. Zakrzewska, T. Daniluk, E. Piktel, S. Chmielewska, R. Bucki, Two lineages of *Pseudomonas aeruginosa* filamentous phages: Structural uniformity over integration preferences. *Genome Biol. Evol.* **12**, 1765–1781 (2020).
19. E. B. Burgener, P. R. Secor, M. C. Tracy, J. M. Sweere, E. M. Bik, C. E. Milla, P. L. Bollyky, Methods for extraction and detection of Pf bacteriophage dna from the sputum of patients with cystic fibrosis. *Phage* **1**, 100–108 (2020).
20. E. M. Waters, D. R. Neill, B. Kaman, J. S. Sahota, M. R. J. Clokie, C. Winstanley, A. Kadioglu, Phage therapy is highly effective against chronic lung infections with *Pseudomonas aeruginosa*. *Thorax* **72**, 666–667 (2017).
21. S. Trend, A. M. Fonceca, W. G. Ditcham, A. Kicic, A. Cf, The potential of phage therapy in cystic fibrosis: Essential human-bacterial-phage interactions and delivery considerations for use in *Pseudomonas aeruginosa*-infected airways. *J. Cyst. Fibros.* **16**, 663–670 (2017).
22. I. D. Hay, T. Lithgow, Filamentous phages: Masters of a microbial sharing economy. *EMBO Rep.* **20**, (2019).
23. J. S. Webb, M. Lau, S. Kjelleberg, Bacteriophage and phenotypic variation in *Pseudomonas aeruginosa* biofilm development. *J. Bacteriol.* **186**, 8066–8073 (2004).
24. P. R. Secor, E. B. Burgener, M. Kinnersley, L. K. Jennings, V. Roman-Cruz, M. Popescu, J. D. Van Belleghem, N. Haddock, C. Copeland, L. A. Michaels, C. R. de Vries, Q. Chen, J. Pourtois, T. J. Wheeler, C. E. Milla, P. L. Bollyky, Pf bacteriophage and their impact on *Pseudomonas* virulence, mammalian immunity, and chronic infections. *Front. Immunol.* **11**, 244 (2020).
25. S. A. Rice, C. H. Tan, P. J. Mikkelsen, V. Kung, J. Woo, M. Tay, A. Hauser, D. McDougald, J. S. Webb, S. Kjelleberg, The biofilm life cycle and virulence of *Pseudomonas aeruginosa* are dependent on a filamentous prophage. *ISME J.* **3**, 271–282 (2009).
26. P. R. Secor, J. M. Sweere, L. A. Michaels, A. V. Malkovskiy, D. Lazzareschi, E. Katznelson, J. Rajadas, M. E. Birnbaum, A. Arrigoni, K. R. Braun, S. P. Evanko, D. A. Stevens, W. Kaminsky, P. K. Singh, W. C. Parks, P. L. Bollyky, Filamentous bacteriophage promote biofilm assembly and function. *Cell Host Microbe* **18**, 549–559 (2015).
27. M. Brown-Jaque, L. Rodriguez Oyarzun, T. Cornejo-Sanchez, M. T. Martin-Gomez, S. Gartner, J. de Gracia, S. Rovira, A. Alvarez, J. Jofre, J. J. Gonzalez-Lopez, M. Muniesa, Detection of bacteriophage particles containing antibiotic resistance genes in the sputum of cystic fibrosis patients. *Front. Microbiol.* **9**, 856 (2018).
28. E. B. Burgener, J. M. Sweere, M. S. Bach, P. R. Secor, N. Haddock, L. K. Jennings, R. L. Marvig, H. K. Johansen, E. Rossi, X. Cao, L. Tian, L. Nedelec, S. Molin, P. L. Bollyky, C. E. Milla, Filamentous bacteriophages are associated with chronic *Pseudomonas* lung infections and antibiotic resistance in cystic fibrosis. *Sci. Transl. Med.* **11**, eaau9748 (2019).
29. M. S. Bach, C. R. de Vries, A. Khosravi, J. M. Sweere, M. C. Popescu, Q. Chen, S. Demirdjian, A. Hargil, J. D. Van Belleghem, G. Kaber, M. Hajfathalian, E. B. Burgener, D. Liu, Q. L. Tran, T. Dharmaraj, M. Birukova, V. Sunkari, S. Balaji, N. Ghosh, S. S. Mathew-Steiner, M. S. El Masry, S. G. Keswani, N. Banaei, L. Nedelec, C. K. Sen, V. Chandra, P. R. Secor, G. A. Suh, P. L. Bollyky, Filamentous bacteriophage delays healing of *Pseudomonas*-infected wounds. *Cell. Rep. Med.* **3**, 100656 (2022).
30. Q. Chen, T. Dharmaraj, P. C. Cai, E. B. Burgener, N. L. Haddock, A. J. Spakowitz, P. L. Bollyky, Bacteriophage and bacterial susceptibility, resistance, and tolerance to antibiotics. *Pharmaceutics* **14**, 1425 (2022).
31. A. K. Tarafder, A. von Kugelgen, A. J. Mellul, U. Schulze, D. Aarts, T. A. M. Bharat, Phage liquid crystalline droplets form occlusive sheaths that encapsulate and protect infectious rod-shaped bacteria. *Proc. Natl. Acad. Sci. U.S.A.* **117**, 4724–4731 (2020).
32. J. Böhning, M. Ghrayeb, C. Pedebos, D. K. Abbas, S. Khalid, L. Chai, T. A. M. Bharat, Donor-strand exchange drives assembly of the TasA scaffold in Bacillus subtilis biofilms. *Nat. Commun.* **13**, 7082 (2022).
33. M. T. van Rossem, S. Wilks, P. R. Secor, M. Kaczmarek, G. D'Alessandro, Homogenization modelling of antibiotic diffusion and adsorption in viral liquid crystals. *R. Soc. Open Sci.* **10**, 221120 (2023).
34. M. van Rossem, S. Wilks, M. Kaczmarek, P. R. Secor, G. D'Alessandro, Modelling of filamentous phage-induced antibiotic tolerance of *P. aeruginosa*. *PLOS ONE* **17**, e0261482 (2022).
35. S. Kirchner, J. L. Fothergill, E. A. Wright, C. E. James, E. Mowat, C. Winstanley, Use of artificial sputum medium to test antibiotic efficacy against *Pseudomonas aeruginosa* in conditions more relevant to the cystic fibrosis lung. *J. Vis. Exp.*, e3857 (2012).
36. K. R. Purdy Drew, L. K. Sanders, Z. W. Culumber, O. Zribi, G. C. Wong, Cationic amphiphiles increase activity of aminoglycoside antibiotic tobramycin in the presence of airway polyelectrolytes. *J. Am. Chem. Soc.* **131**, 486–493 (2009).
37. D. Priftis, N. Laugel, M. Tirrell, Thermodynamic characterization of polypeptide complex coacervation. *Langmuir* **28**, 15947–15957 (2012).
38. A. B. Kayitmazer, Thermodynamics of complex coacervation. *Adv. Colloid Interface Sci.* **239**, 169–177 (2017).
39. D. Priftis, K. Megley, N. Laugel, M. Tirrell, Complex coacervation of poly(ethylene-imine)/polypeptide aqueous solutions: Thermodynamic and rheological characterization. *J. Colloid Interface Sci.* **398**, 39–50 (2013).
40. M. K. Bhattacharyya, P. G. Devi, D. Dasgupta, S. J. Bora, B. K. Das, Solid and solution structures and DNA binding properties of $[M^{II}(4\text{-}CNpy)_2(SO_4)(H_2O)_3]\cdot H_2O$ for M=Cu, Co, Ni. *Polyhedron* **35**, 62–68 (2012).
41. A. H. Alkhzem, T. J. Woodman, I. S. Blagbrough, Individual pK_a values of tobramycin, kanamycin B, amikacin, sisomicin, and netilmicin determined by multinuclear NMR spectroscopy. *ACS Omega* **5**, 21094–21103 (2020).
42. D. McShane, J. C. Davies, M. G. Davies, A. Bush, D. M. Geddes, E. W. Alton, Airway surface pH in subjects with cystic fibrosis. *Eur. Respir. J.* **21**, 37–42 (2003).
43. Y. Xie, L. Lu, X. X. Tang, T. O. Moninger, T. J. Huang, D. A. Stoltz, M. J. Welsh, Acidic submucosal gland pH and elevated protein concentration produce abnormal cystic fibrosis mucus. *Dev. Cell* **54**, 488–500.e5 (2020).
44. P. A. Janmey, D. R. Slochower, Y. H. Wang, Q. Wen, A. Cebers, Polyelectrolyte properties of filamentous biopolymers and their consequences in biological fluids. *Soft Matter* **10**, 1439–1449 (2014).
45. Y. Herasimenka, M. Benincasa, M. Mattiuzzo, P. Cescutti, R. Gennaro, R. Rizzo, Interaction of antimicrobial peptides with bacterial polysaccharides from lung pathogens. *Peptides* **26**, 1127–1132 (2005).
46. S. Sandgren, A. Wittrup, F. Cheng, M. Jonsson, E. Eklund, S. Busch, M. Belting, The human antimicrobial peptide LL-37 transfers extracellular DNA plasmid to the nuclear compartment of mammalian cells via lipid rafts and proteoglycan-dependent endocytosis. *J. Biol. Chem.* **279**, 17951–17956 (2004).
47. Y. Lai, S. Adhikarakunnathu, K. Bhardwaj, C. T. Ranjith-Kumar, Y. Wen, J. L. Jordan, L. H. Wu, B. Dragnea, L. San Mateo, C. C. Kao, LL37 and cationic peptides enhance TLR3 signaling by viral double-stranded RNAs. *PLOS ONE* **6**, e26632 (2011).
48. T. Seviour, F. R. Winnerdy, L. L. Wong, X. Shi, S. Mugunthan, Y. H. Foo, R. Castaing, S. S. Adav, S. Subramoni, G. S. Kohli, H. M. Shewan, J. R. Stokes, S. A. Rice, A. T. Phan, S. Kjelleberg, The biofilm matrix scaffold of *Pseudomonas aeruginosa* contains G-quadruplex extracellular DNA structures. *NPJ Biofilms Microbiomes* **7**, 27 (2021).
49. L. Turnbull, M. Toyofuku, A. L. Hynen, M. Kurosawa, G. Pessi, N. K. Petty, S. R. Osvath, G. Carcamo-Oyarce, E. S. Gloag, R. Shimoni, U. Omasits, S. Ito, X. Yap, L. G. Monahan, R. Cavaliere, C. H. Ahrens, I. G. Charles, N. Nomura, L. Eberl, C. B. Whitchurch, Explosive cell lysis as a mechanism for the biogenesis of bacterial membrane vesicles and biofilms. *Nat. Commun.* **7**, 11220 (2016).
50. T. C. Piva, C. Luft, K. H. Antunes, P. J. C. Marostica, L. A. Pinto, M. V. F. Donadio, Extracellular DNA in sputum is associated with pulmonary function and hospitalization in patients with cystic fibrosis. *Respir. Med.* **172**, 106144 (2020).
51. J. M. Sweere, J. D. Van Belleghem, H. Ishak, M. S. Bach, M. Popescu, V. Sunkari, G. Kaber, R. Manasherob, G. A. Suh, X. Cao, C. R. de Vries, D. N. Lam, P. L. Marshall, M. Birukova, E. Katznelson, D. V. Lazzareschi, S. Balaji, S. G. Keswani, T. R. Hawn, P. R. Secor, P. L. Bollyky, Bacteriophage trigger antiviral immunity and prevent clearance of bacterial infection. *Science* **363**, eaat9691 (2019).

Acknowledgments

Funding: This project is supported by NIH R01AI138981. Q.C. is supported by Cystic Fibrosis Foundation CHEN21F0 and Stanford Maternal and Child Health Research Institute. P.C. is supported by National Science Foundation Graduate Research Fellowship Program (NSF-GRFP). Financial support for A.J.S. is provided by the National Science Foundation, Physics of Living Systems Program (PHY-2102726). E.B. acknowledges funding from Cystic Fibrosis Foundation and Harry Shwachman Award. A.E.B. is supported by NIH 1DP1 OD029517-01. A.E.B. also acknowledges funding from Stanford University's Discovery Innovation Fund, from the Cisco University Research Program Fund and the Silicon Valley Community Foundation, and from Dr. James J. Truchard and the Truchard Foundation. J.E.N. was funded by grant NNF21OC0068675 from the Novo Nordisk Foundation and the Stanford Bio-X Program. C.M. acknowledges funding from NIH R01 HL148184 and Ross Mosier CF Research Laboratories Research Fund. **Author contributions:** Conceptualization: P.L.B., M.J.K., Q.C., P.C., A.S., E.B., and C.M. Methodology: Q.C., P.C., T.H.W.C., M.J.K., P.L.B., and A.S. Investigation: Q.C., P.C., T.H.W.C., A.G., and A.H. Visualization: Q.C. and P.C. Supervision: P.L.B., A.S., C.M., and S.C.H. Writing—

original draft: Q.C. and P.C. Writing—review and editing: Q.C., P.C., E.B., P.L.B., A.S., C.M., P.R.C, J.E.N, A.E.B., and S.C.H. **Competing interests:** The authors declare that they have no competing interests. **Data and materials availability:** All data needed to evaluate the conclusions in the paper are present in the paper and/or the Supplementary Materials.

Submitted 26 October 2023
Accepted 30 April 2024
Published 31 May 2024
10.1126/sciadv.adl5576